First-principles calculations on the elastic and thermodynamic properties of NbN*

Ren Da-Hua(任达华) and Cheng Xin-Lu(程新路)†

Institute of Atomic and Molecular Physics, Sichuan University, Chengdu 610065, *China*

(Received 12 April 2012; revised manuscript received 16 May 2012)

The elastic and thermodynamic properties of NbN at high pressures and high temperatures are investigated by the plane-wave pseudopotential density functional theory (DFT). The generalized gradient approximation (GGA) with the Perdew–Burke–Ernzerhof (PBE) method is used to describe the exchange–correlation energy in the present work. The calculated equilibrium lattice constant a_0, bulk modulus B_0, and the pressure derivative of bulk modulus B_0' of NbN with rocksalt structure are in good agreement with numerous experimental and theoretical data. The elastic properties over a range of pressures from 0 to 80.4 GPa are obtained. Isotropic wave velocities and anisotropic elasticity of NbN are studied in detail. It is indicated that NbN is highly anisotropic in both longitudinal and shear-wave velocities. According to the quasi-harmonic Debye model, in which the phononic effect is considered, the relations of $(V - V_0)/V_0$ to the temperature and the pressure, and the relations of the heat capacity C_V and the thermal expansion coefficient α to temperature are discussed in a pressure range from 0 to 80.4 GPa and a temperature range from 0 to 2500 K. At low temperature, C_V is proportional to T^3 and tends to the Dulong–Petit limit at higher temperature. We predict that the thermal expansion coefficient α of NbN is about 4.20×10^{-6}/K at 300 K and 0 GPa.

Keywords: NbN density functional theory, quasi-harmonic Debye model, elastic constants, thermodynamic properties

PACS: 71.15.Mb, 62.20.de, 67.25.bd **DOI:** 10.1088/1674-1056/21/12/127103

1. Introduction

Transition-metal (TM) nitrides have increasingly attracted attention theoretically and experimentally because of their outstanding mechanical, optoelectronic, thermal, semiconducting, magnetic or superconducting properties, which can be used advantageously in a variety of technological areas.[1−5] Furthermore, their high hardness plays an important role in applications; considerable efforts have been devoted to investigating their mechanical properties.[6−14] The special physical properties of niobium nitride make it a suitable material exploited in superconducting and high hardness coatings.[15,16] To study the mechanical properties of NbN, the hardness measurements have been performed by Vickers indentation method, and its Vickers hardness is close to that of sapphire, while its bulk modulus approaches that of cubic boron nitride.[6,7] Amriou *et al.*[13] have investigated the electronic structures and bonding mechanisms of NbC and NbN compounds using the full-potential linearized augmented plane wave method (FP-LAPW). Wang *et al.*[14] have studied the mechanical properties of NbN with the density functional theory (DFT), which provides important insights into the physical origin of the mechanical properties. However, to our knowledge, even though NbN has been well known for a long time, calculations on the elastic and thermodynamic properties of NbN have not been reported. In the present work, we investigate the elastic and thermodynamic properties of NbN by DFT combined with the quasi-harmonic Debye model.

2. Computational method

We investigate the structural, elastic, and thermodynamic properties of NbN by using DFT and combining the quasi-harmonic Debye model.[17] Vanderbilt-type ultrasoft pseudopotential[18] is employed to perform the interactions of electrons with atoms for Nb $4s^2 4p^6 4d^4 5s^1$ and N $2s^2 2p^3$. The generalized gradient approximation (GGA) with Perdew–Burke–Ernzerhof (PBE)[19] is used to describe the exchange and correlation energy. The plane-wave basis set with an energy cutoff of 430 eV is adopted. The special point sampling integration over the Brillouin zone is based on the Monkhorst–Pack method[20] with $6 \times 6 \times 6$ k-point mesh points, where the self-consistent convergence of the total energy is about 2.0×10^{-5} eV/atom,

*Project supported by the National Natural Science Foundation of China (Grant No. 11176020).

†Corresponding author. E-mail: chengxl@scu.edu.cn

© 2012 Chinese Physical Society and IOP Publishing Ltd

the maximum atom force is less than 0.05 eV/Å (1 Å=0.1 nm), the maximum atoms displacement is less than 1.0×10^{-5} Å, and the maximum stress is within 0.01 GPa. All the total energy calculations are performed using the Cambridge Serial Total Energy Package (CASTEP) code.[21,22]

3. Results and discussion

3.1. Structure of NbN

By checking the ICSD crystal database, we present the basic crystal parameters of NbN as follows: the space group is $Fm\bar{3}m$ (225#) with rocksalt structure, the atomic site of Nb is 4*a* (0, 0, 0) and N is 4*b* (1/2, 1/2, 1/2). The ground state lattice parameter a_0 for the rocksalt structure of NbN is obtained by optimizing the geometry, and the total energy E and the corresponding primitive cell volume V are calculated by setting a series of different lattice constants. Then we obtain the zero pressure bulk modulus B_0 and its pressure derivative B_0' by fitting the E–V curve with the Brich–Murnaghan equation of state (EOS).[23] All calculated results are listed in Table 1. It is indicated that our results are in excellent agreement with numerous theoretical[13,14,24–31] and experimental[1,32–34] data. The calculated method performed in the present work is reasonable.

Table 1. Values of lattice constant a_0 (Å), bulk modulus B_0 (GPa), pressure derivative B_0' (GPa), and elastic constants C_{11}, C_{12}, C_{44} (GPa) for NbN at zero pressure.

	a_0/Å	B_0/GPa	B_0'/GPa	C_{11}/GPa	C_{12}/GPa	C_{44}/GPa
Present work	4.415	307.2	4.416	696.2	112.6	85.9
Ref. [14]	4.410	313.0	–	–	–	–
Ref. [24]	4.410	309.0	–	–	–	–
Ref. [25]	4.394	–	–	–	–	–
Ref. [26]	4.420	317.0	–	–	–	–
Ref. [27]	4.378	–	–	–	–	–
Ref. [28]–[30]	4.392	–	–	–	–	–
Ref. [31]	–	350.0	–	–	–	–
Ref. [13]	4.430 (GGA)	307.4	4.214	498.0	212.0	89.0
	4.363 (LDA)	349.9	4.922	604.0	223.0	184.0
Ref. [1]	4.390	320.0	–	–	–	–
Ref. [32]	–	287.0	–	556.0	152.0	125.0
Ref. [33]	4.379	292.0 354.0	–	–	–	–
Ref. [34]	4.393	–	–	–	–	–

3.2. Elastic properties of NbN

According to Hooke's law,[35] the stress (σ) and strain (ε) for small deformation to a crystal are linearly related by

$$\sigma_{ij} = c_{ijkl}\varepsilon_{kl} \ (i,j,k,l = 1,2,3), \tag{1}$$

where the fourth-rank tensor c_{ijkl} is the elastic constant tensor. To calculate the elastic constants we use the finite strain method and then the elastic constants can be determined directly from the stress generated by small strain.[36] For the cubic crystal, there are only three independent elastic constants, namely, C_{11}, C_{12}, and C_{44}. The strained lattice vector $\boldsymbol{a}'$ is used to determine the elastic constants versus the unstrained lattice vector $\boldsymbol{a}$ by $\boldsymbol{a}' = (I + \varepsilon)\boldsymbol{a}$, where I is the identity matrix. The strain tensor is

$$\varepsilon = \begin{pmatrix} e & e/2 & 0 \\ e/2 & 0 & 0 \\ 0 & 0 & 0 \end{pmatrix} \tag{2}$$

so Hooke's law is expressed as follows:

$$\sigma_{xx} = C_{11}e, \quad \sigma_{yy} = \sigma_{zz} = C_{12}e,$$
$$\sigma_{yz} = C_{44}e, \quad \sigma_{zx} = \sigma_{xy} = 0. \tag{3}$$

Obtaining the equilibrium primitive cell of NbN by optimizing the geometry, a series of incremental strains is applied to the crystal. At each step of strain, only electrons can be relaxed while atomic positions and the atomic basis vector orthogonal to the applied

strain are fixed by the symmetry. Then the strain-induced stresses are calculated and the values of C_{11}, C_{12}, and C_{44} for NbN are determined by Eq. (3).

The ratio of stress to strain versus strain is plotted in Fig. 1. The different strain magnitudes: $e = 0.02$, $e = 0.04$, $e = 0.06$, $e = 0.08$, $e = 0.10$ are used to deform the equilibrium primitive of NbN. From the intercept of the best-fit line: $\sigma_{xx}/e = C_{11} + A(e)$, the values of C_{11}, C_{12}, and C_{44} are successfully obtained to be $C_{11} = 696.2$ GPa, $C_{12} = 112.6$ GPa, and $C_{44} = 85.9$ GPa at zero pressure. We repeat this method of stress-induced strain and calculate the values of C_{11}, C_{12}, and C_{44} at different pressures. The elastic constants completely specify the elastic properties and acoustic velocities of a single crystal.

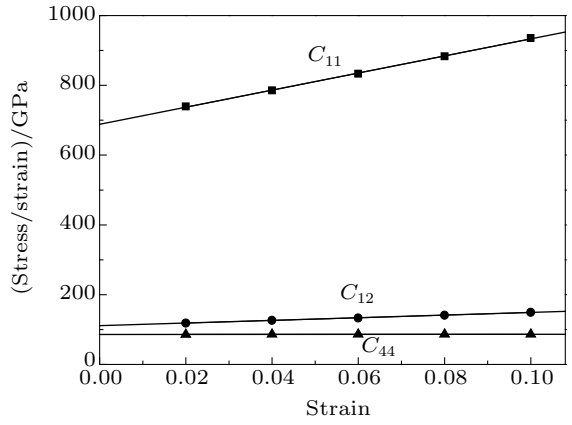


Fig. 1. Stress/strain ratios versus strain. The solid lines represent linear fittings to the calculated values (solid circles) of stress/strains versus strain for three independent stiffness constants.

As is well known, the mechanical stability for a cubic crystal under isotropic pressure is judged by the following conditions[37]

$$\tilde{C}_{\alpha\alpha} > 0,\ \tilde{C}_{11} > |\tilde{C}_{12}|,\ \tilde{C}_{11} + 2\tilde{C}_{12} > 0, \qquad (4)$$

where $\tilde{C}_{\alpha\alpha} = C_{\alpha\alpha} - P(\alpha = 1, 4)$, $\tilde{C}_{12} = C_{12} + P$.

The calculated results indicate that when the pressure is less than 80.4 GPa, the elastic constants of NbN satisfy Eq. (4); namely, the structure of NbN should be stable under these conditions. According to the previous study, there is no structural phase transition for NbN at the temperatures up to 2500 K.[38] Then, we investigate the elastic and thermodynamic properties of NbN in a pressure range from 0 to 80.4 GPa and a temperature range from 0 to 2500 K. In the case of hydrostatic pressure P, the shear modulus G and bulk modulus B are related to the elastic constants C_{ij} as follows:[39,40]

$$G = (G_{\rm V} + G_{\rm R})/2,\ B = (C_{11} + 2C_{12})/3, \qquad (5)$$

where $c' = (C_{11} - C_{12})/2$, $G_{\rm V} = (2c' + 3C_{44})/5$, $G_{\rm R} = 15/(6/c' + 9/C_{44})$, B is the bulk modulus, $G_{\rm V}$ is the Voigt shear modulus and $G_{\rm R}$ is the Reuss shear modulus. The results are listed in Table 2. The elastic constants C_{ij} and bulk modulus B at different pressures and temperatures are shown in Figs. 2(a) and 2(b). The elastic constants and bulk modulus increase with increasing pressure and decrease with rising temperature. It is found that C_{11} and C_{12} increase with increasing pressure; the variation of C_{11} is obvious compared with that of C_{12}, but the variation of C_{44} is very slight. The elastic constant C_{11} represents elasticity in length. A longitudinal strain produces a change in C_{11}. The elastic constants C_{12} and C_{44} are related to the elasticity in shape, which is a shear constant. A transverse strain causes a change in shape but not in volume. For cubic crystals, there are two shear moduli, c and c', corresponding to the shears along the {100} and {110} planes, respectively, which

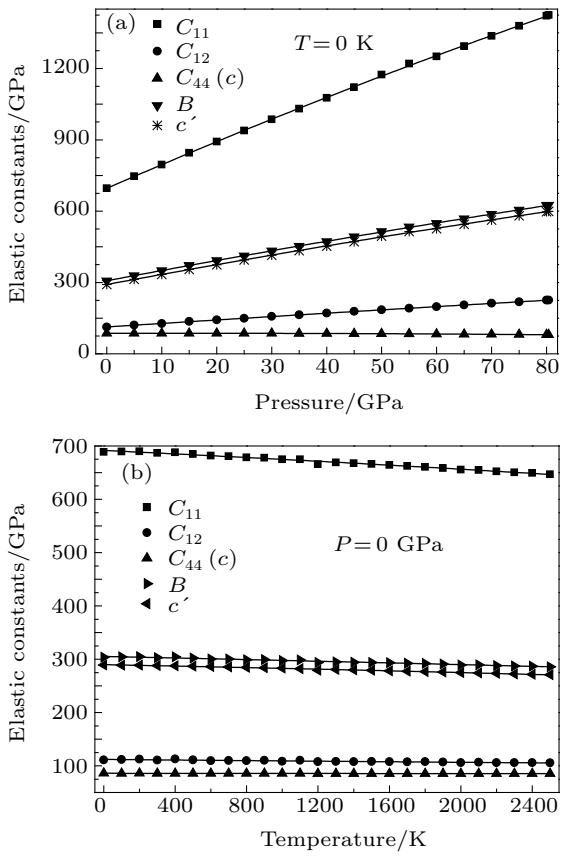


Fig. 2. Elastic constants versus pressure at $T = 0$ K (a), and bulk moduli versus temperature at $P = 0$ GPa (b).

can be used to estimate distortion in a certain plane of NbN as follows:

$$c = C_{44},\ c' = \frac{1}{2}(C_{11} - C_{12}). \tag{6}$$

As shown in Figs. 2(a) and 2(b), c varies just a little with temperature and pressure, which shows that pressure and temperature will not cause obvious variation of shear along the {100} plane. At the same time, c' varies substantially with the increase of pressure, indicating that pressure will make the shear change along the {110} plane. The change in c' is inversely proportional to temperature, but the amplitude of variation is very small. The bulk modulus B reflects the extent of difficulty of material compression under hydrostatic pressure. Therefore, compressibility of NbN is low at high pressure ($T = 0$ K), and large at high temperature ($P = 0$ GPa).

Table 2. Values of the lattice constant (Å), density (g·cm^{-3}), elastic moduli (GPa), wave velocities (km·s^{-1}), and Debye temperature (K) for NbN from 0 to 80.4 GPa at different pressures.

P	a	ρ	C_{11}	C_{12}	C_{44}	B	$G_{\rm V}$	$G_{\rm R}$	G	$v_{\rm P}$	$v_{\rm S}$	$\Theta_{\rm D}$
0	4.415	8.250	696.2	112.6	85.9	696.2	168.3	119.7	144.0	7.78	4.18	629.1
5	4.392	8.379	746.5	120.4	86.2	746.5	176.9	121.4	149.2	7.94	4.22	639.2
10	4.371	8.504	795.5	127.3	86.4	795.5	185.5	122.8	154.1	8.08	4.26	648.5
15	4.351	8.623	845.1	135.7	86.5	845.1	193.8	124.0	158.9	8.23	4.29	657.3
20	4.332	8.736	892.3	142.7	86.4	892.3	201.8	124.9	163.3	8.36	4.32	665.4
25	4.314	8.844	938.5	149.2	86.3	938.5	209.6	125.6	167.6	8.48	4.35	673.0
30	4.297	8.951	985.6	156.8	86.1	985.6	217.4	126.0	171.7	8.60	4.38	680.2
35	4.281	9.052	1031.0	163.6	85.8	1031.0	224.9	126.3	175.6	8.71	4.40	686.9
40	4.265	9.151	1076.3	170.7	85.5	1076.3	232.4	126.5	179.5	8.82	4.43	693.4
45	4.251	9.246	1121.3	178.0	85.0	1121.3	239.7	126.5	183.1	8.93	4.45	699.5
50	4.237	9.338	1174.4	184.6	84.5	1174.4	248.6	126.4	187.5	9.05	4.48	707.0
55	4.223	9.427	1220.1	191.5	83.9	1220.1	256.1	126.2	191.1	9.15	4.50	712.9
60	4.210	9.515	1250.3	197.9	83.4	1250.3	260.5	125.7	193.1	9.20	4.50	715.6
65	4.198	9.601	1293.9	205.3	82.6	1293.9	267.2	125.0	196.1	9.30	4.52	720.4
70	4.186	9.684	1336.6	212.1	81.9	1336.6	274.0	124.4	199.2	9.38	4.54	725.3
75	4.174	9.766	1378.8	218.4	81.3	1378.8	280.9	124.0	202.4	9.47	4.55	730.3
80	4.163	9.845	1421.3	225.4	80.5	1421.3	287.4	123.1	205.3	9.55	4.57	734.6
80.4	4.162	9.852	1424.4	225.7	80.5	1424.4	288.0	123.0	205.5	9.55	4.57	735.0

3.3. Isotropic wave velocities

We calculate the longitudinal and shear-wave velocities, $v_{\rm P}$ and $v_{\rm S}$ respectively, which are obtained from Navier's equation[41]

$$v_{\rm P} = \sqrt{\frac{B + \frac{4}{3}G}{\rho}},\ \text{and}\ v_{\rm S} = \sqrt{\frac{G}{\rho}}, \tag{7}$$

where ρ is the density of NbN. The calculated densities and wave velocities at different pressures are shown in Table 2, and the plots of $v_{\rm P}$ and $v_{\rm S}$ versus pressure are shown in Fig. 3. The longitudinal and shear-wave velocities, $v_{\rm P}$ and $v_{\rm S}$, increase with the increase of pressure. However, the longitudinal wave velocity increases more obviously than shear-wave velocity with the increase of pressure. The high-pressure (80.4 GPa) longitudinal and shear-wave velocities for NbN differ by 22.8% and 9.3% from those at zero-pressure.

The averaged sound velocity can be computed using the above two equations and can be defined as[42]

$$v_{\rm m} = \left[\frac{1}{3}\left(\frac{2}{v_{\rm S}^3} + \frac{1}{v_{\rm P}^3}\right)\right]^{-1/3}. \tag{8}$$

Thus, the Debye temperature, which is proportional to the averaged sound velocity, can be calculated from the following equation:[43]

$$\Theta_{\rm D} = \frac{h}{k}\left[\frac{3n}{4\pi}\left(\frac{N_{\rm A}\rho}{M}\right)\right]^{1/3} v_{\rm m}, \tag{9}$$

where h is the Planck's constant, k is the Boltzmann's constant, $N_{\rm A}$ is the Avogadro's number, n is the num-

ber of atoms in the molecule, M is the molecular weight and ρ is the density. At 0 K, using the above method, we obtain $\Theta_{\rm D} = 629.1$ K. The Debye temperature $\Theta_{\rm D}$ increases monotonically with pressure increasing (see Table 2).

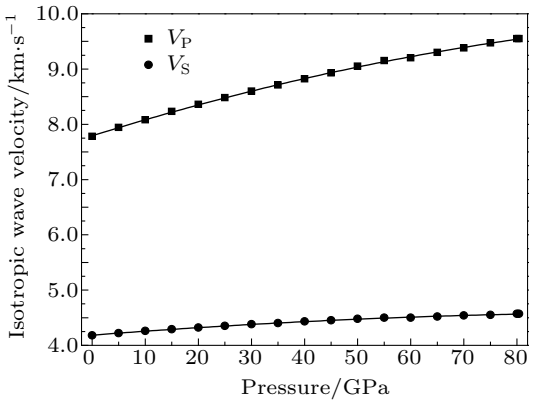


Fig. 3. The isotropic longitudinal and shear-wave velocities of NbN versus pressure.

3.4. Elastic anisotropy

The acoustic vibrational modes of a solid in the long wavelength limit are obtained from the Christoffel equation,[44]

$$\rho\omega^2 u_i = M_{il}u_l, \tag{10}$$

where ρ is the mass density, ω is the vibrational angular frequency, u_i is the displacement amplitude and summation convention is used for repeated Cartesian indices. The matrix M_{il} is given by

$$M_{il} = c_{ijkl}k_j k_k, \tag{11}$$

where c_{ijkl} is the elastic constant tensor element, and k_j is the wave vector component of the vibrational wave. In the case of the cubic crystal, the M_{il} matrix reduces to

$$\begin{bmatrix} C_{11}k_x^2 + (k_y^2 + k_z^2)C_{44} & (C_{12} + C_{44})k_x k_y & (C_{12} + C_{44})k_x k_z \\ (C_{12} + C_{44})k_x k_y & C_{11}k_y^2 + (k_x^2 + k_z^2)C_{44} & (C_{12} + C_{44})k_y k_z \\ (C_{12} + C_{44})k_x k_z & (C_{12} + C_{44})k_y k_z & C_{11}k_z^2 + (k_x^2 + k_y^2)C_{44} \end{bmatrix}. \tag{12}$$

For any direction, the eigenvector will be a quadratic function of $k = |\boldsymbol{k}|$ and hence $\omega = V_n(\hat{k})k$ with $V_n(\hat{k})$ being the sound velocity for polarization n and direction $\hat{k}$. For example, for $\boldsymbol{k}$ along [100], $k_x = 1$ and $k_y = k_z = 0$, the sound velocities become

$$\begin{aligned} V_{\rm P}([100]) &= \sqrt{C_{11}/\rho}, \\ V_{\rm S1}([100]) &= V_{\rm S2}([100]) = \sqrt{C_{44}/\rho}, \end{aligned} \tag{13}$$

where $V_{\rm P}$ is longitudinal velocity; $V_{\rm S1}$ and $V_{\rm S2}$ are shear-wave velocities polarized in the $(\bar{1}10)$ plane (S1) and (001) plane (S2) along propagation direction [100], respectively.

Similarly, for the [110] wave vector direction, the sound velocities are given by the results

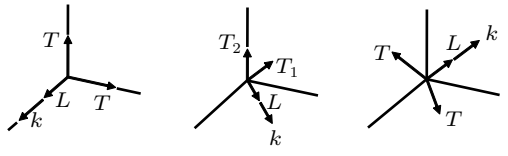
$$\begin{aligned} V_{\rm P}([110]) &= \sqrt{\frac{1}{2}(C_{11} + C_{12} + 2C_{44})/\rho}, \\ V_{\rm S1}([110]) &= \sqrt{\frac{1}{2}(C_{11} - C_{12})/\rho}, \\ V_{\rm S2}([110]) &= \sqrt{C_{44}/\rho}, \end{aligned} \tag{14}$$

where $V_{\rm P}$ is the longitudinal velocity; $V_{\rm S1}$ and $V_{\rm S2}$ are the shear-wave velocities polarized in the $(\bar{1}10)$ plane (S1) and (001) plane (S2) along propagation direction [110], respectively.

And for the [111] wave vector direction

$$\begin{aligned} V_{\rm P}([111]) &= \sqrt{\frac{1}{3}(C_{11} + 2C_{12} + 4C_{44})/\rho}, \\ V_{\rm S1}([111]) &= V_{\rm S2}([111]) \\ &= \sqrt{\frac{1}{3}(C_{11} - C_{12}, +C_{44})/\rho}, \end{aligned} \tag{15}$$

where $V_{\rm P}$ is the longitudinal velocity; $V_{\rm S1}$ and $V_{\rm S2}$ are the shear-wave velocities polarized in the $(\bar{1}10)$ plane (S1) and (001) plane (S2) along propagation direction [110], respectively.



k along [100] k along [110] k along [111]

Fig. 4. Longitudinal and transverse waves (two shear waves) on propagation along different directions with wave vector $\boldsymbol{k}$ polarized along directions [100], [110], and [111].

The longitudinal and two shear-efficient elastic constants at different pressures are presented in Table 3. Velocities along different directions are shown in Table 4 and Fig. 4. It is found that NbN is highly

anisotropic in both longitudinal and shear-wave velocities. Longitudinal wave velocities are extremal for [100] and [111] propagation directions, whereas shear waves polarized in the $(\bar{1}10)$ plane (S1) are extremal along [100] and [110]. In addition, shear waves polarized in the (001) plane (S2) show a local extremum in the shear velocity for propagation along [1/2, 1/2, $1/\sqrt{2}$].

Table 3. Longitudinal and two shear-efficient elastic constants (GPa) of wave vectors along [100], [110], and [111] at different pressures.

	C_L	C_{T1}	C_{T2}	C_L	C_{T1}	C_{T2}	C_L	C_{T1}	C_{T2}
		[100]			[110]			[111]	
0	696.2	85.9	85.9	490.3	291.8	85.9	421.7	223.2	223.2
5	746.5	86.2	86.2	519.6	313.1	86.2	444.0	237.4	237.4
10	795.5	86.4	86.4	547.8	334.1	86.4	465.2	251.5	251.5
15	845.1	86.5	86.5	576.9	354.7	86.5	487.4	265.3	265.3
20	892.3	86.4	86.4	603.9	374.8	86.4	507.8	278.7	278.7
25	938.5	86.3	86.3	630.2	394.6	86.3	527.4	291.9	291.9
30	985.6	86.1	86.1	657.3	414.4	86.1	547.8	305.0	305.0
35	1031.0	85.8	85.8	683.1	433.7	85.8	567.1	317.7	317.7
40	1076.3	85.5	85.5	709.0	452.8	85.5	586.5	330.3	330.3
45	1121.3	85.0	85.0	734.7	471.6	85.0	605.8	342.8	342.8
50	1174.4	84.5	84.5	764.0	494.9	84.5	627.2	358.1	358.1
55	1220.1	83.9	83.9	789.7	514.3	83.9	646.3	370.9	370.9
60	1250.3	83.4	83.4	807.5	526.2	83.4	659.9	378.6	378.6
65	1293.9	82.6	82.6	832.2	544.3	82.6	678.2	390.4	390.4
70	1336.6	81.9	81.9	856.3	562.2	81.9	696.2	402.1	402.1
75	1378.8	81.3	81.3	879.9	580.2	81.3	713.6	413.9	413.9
80	1421.3	80.5	80.5	903.8	597.9	80.5	731.3	425.4	425.4
80.4	1424.4	80.4	80.4	905.4	599.3	80.4	732.5	426.4	426.4

Table 4. Values of longitudinal and two shear-wave velocities ($\mathrm{km\cdot s^{-1}}$) in three directions at pressures ranging from 0 to 80.4 GPa.

P	[100]			[110]			[111]			Δ_{P}	Δ_{S}
	V_{P}	V_{S1}	V_{S2}	V_{P}	V_{S1}	V_{S2}	V_{P}	V_{S1}	V_{S2}		
0	9.186	3.227	3.227	7.709	5.947	3.227	7.150	5.201	5.201	25.41	56.77
5	9.439	3.207	3.207	7.875	6.112	3.207	7.279	5.323	5.323	26.34	59.52
10	9.672	3.187	3.187	8.026	6.268	3.187	7.396	5.439	5.439	27.20	62.05
15	9.900	3.167	3.167	8.179	6.414	3.167	7.519	5.547	5.547	27.91	64.40
20	10.106	3.145	3.145	8.315	6.550	3.145	7.624	5.648	5.648	28.59	66.57
25	10.301	3.124	3.124	8.441	6.680	3.124	7.722	5.744	5.744	29.23	68.60
30	10.493	3.101	3.101	8.569	6.804	3.101	7.823	5.837	5.837	29.79	70.56
35	10.672	3.078	3.078	8.687	6.922	3.078	7.915	5.924	5.924	30.33	72.41
40	10.845	3.056	3.056	8.802	7.034	3.056	8.006	6.008	6.008	30.80	74.13
45	11.012	3.033	3.033	8.914	7.142	3.033	8.094	6.089	6.089	31.24	75.80
50	11.214	3.008	3.008	9.045	7.280	3.008	8.195	6.192	6.192	31.83	77.77
55	11.376	2.984	2.984	9.153	7.386	2.984	8.280	6.272	6.272	32.25	79.36
60	11.463	2.960	2.960	9.212	7.436	2.960	8.328	6.308	6.308	32.43	80.39
65	11.609	2.932	2.932	9.310	7.529	2.932	8.405	6.377	6.377	32.78	81.90
70	11.748	2.908	2.908	9.403	7.620	2.908	8.479	6.444	6.444	33.10	83.28
75	11.882	2.886	2.886	9.492	7.708	2.886	8.548	6.510	6.510	33.42	84.58
80	12.015	2.859	2.859	9.581	7.793	2.859	8.619	6.574	6.574	33.72	85.94
80.4	12.024	2.857	2.857	9.587	7.800	2.857	8.623	6.579	6.579	33.75	86.03

Note: $\Delta_{\mathrm{P}} = [(V_{\mathrm{P\,max}} - V_{\mathrm{P\,max}})/V_{\mathrm{Pagg}}] \cdot 100$ and $\Delta_{\mathrm{S}} = [(V_{\mathrm{S\,max}} - V_{\mathrm{S\,max}})/V_{\mathrm{Sagg}}] \cdot 100$.

From the Cristoffel equation[44] for cubic crystal, the elastic anisotropy factor is shown as follows:

$$A = \frac{2C_{44} + C_{12}}{C_{11}} - 1, \tag{16}$$

which is zero for an isotropic material. The anisotropies of P, S1, and S2 waves are then given by

$$A_{\rm P} = \frac{2A}{3}, \quad A_{\rm S1} = -\frac{A}{2}, \quad \text{and} \quad A_{\rm S2} = -\frac{3A}{8}. \tag{17}$$

The pressure dependences of the elastic anisotropic factor A at pressures up to 80.4 GPa are shown in Fig. 5, from which we can know that NbN exhibits low elastic anisotropy at zero pressure and the degree of the anisotropy increases with pressure rising, and the anisotropy factor $A = -0.59$, close to -0.62[33] at zero pressure. The anisotropy factor A initially drops slowly with pressure rising, and then more slowly decreases at higher pressures. The $A_{\rm P}$ decreases more slowly with pressure increasing than A, at the same time, the variations of $A_{\rm S1}$ and $A_{\rm S2}$ are inverse. The above relations (Eq. (17)) explain the corresponding pressure-induced variations in the directions and polarizations of P and S waves with extremal velocities. Both at zero pressure and at high pressure, P waves are fastest along [100] and S waves are fastest along [110] (Table 4).

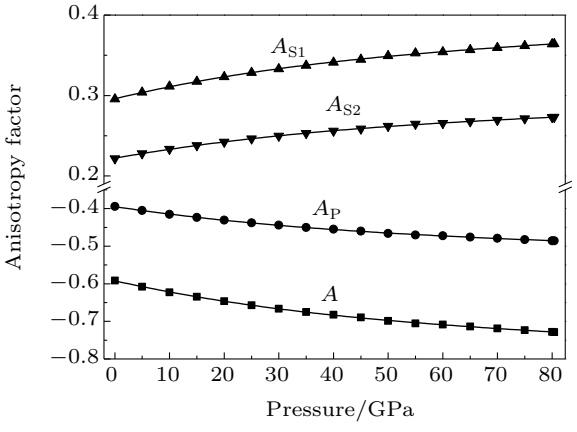


Fig. 5. Anisotropy factors, A, $A_{\rm P}$, $A_{\rm S1}$, and $A_{\rm S2}$ versus pressure for NbN.

3.5. Thermodynamic properties

In order to investigate thermodynamic properties of NbN, the quasi-harmonic Debye model[17] is employed, the non-equilibrium Gibbs function $G^*(V; P, T)$ of NbN is written as

$$G^*(V; P, T) = E(V) + PV + A_{\rm vib}(\Theta(V); T), \tag{18}$$

where $\Theta(V)$ is the Debye temperature and $A_{\rm vib}$ is the vibrational Helmholtz free energy. Considering the phonon effect, introducing the quasi-harmonic approximation[17] and using the Debye model of phonon density of states, $A_{\rm vib}$ can be expressed as follows:[17,45–47]

$$A_{\rm vib}(\Theta; T) = nKT\Big[\frac{9}{8}\frac{\Theta}{T} + 3\ln(1 - {\rm e}^{-\Theta/T}) - D\Big(\frac{\Theta}{T}\Big)\Big], \tag{19}$$

where $(D\Theta/T)$ represents the Debye integral and n is the number of atoms per formula unit. For an isotropic solid, Θ can be written as[46]

$$\Theta = \frac{\hbar}{K}\left[6\pi^2 V^{1/2} n\right]^{1/3} f(\sigma)\sqrt{\frac{B_{\rm S}}{M}}, \tag{20}$$

where M is the molecular mass per formula unit, $f(\sigma)$ is given in Refs. [48] and [49], Poisson ratio $\sigma = 0.25$,[50] $B_{\rm S}$ is the adiabatic bulk modulus approximated by the static compressibility and expressed as[17]

$$B_{\rm S} \approx B(V) = V\Big(\frac{{\rm d}^2 E(V)}{{\rm d}V^2}\Big). \tag{21}$$

The heat capacity $C_{\rm V}$ and the thermal expansion coefficient α are given by[51]

$$C_{\rm V} = 3nk\Big[4D\Big(\frac{\Theta}{T}\Big) - \frac{3\Theta/T}{\exp(\Theta/T) - 1}\Big], \tag{22}$$

$$\alpha = \frac{\gamma C_{\rm V}}{B_T V}, \tag{23}$$

where γ is the Grüneisen parameter. Fortunately, this method is successfully used to investigate the thermodynamic properties of other materials.[52–56]

The thermodynamic properties are determined in a temperature range from 0 to 2500 K, where the quasi-harmonic model remains fully valid. The pressure effect is studied in a 0 GPa–80.4 GPa range. The relations between $(V - V_0)/V_0$ and the pressure at different temperatures are shown in Fig. 6(a) and the variations of $(V - V_0)/V$ with temperature at different pressures are displayed in Fig. 6(b). The positive values of $(V - V_0)/V$ mean that the primitive cell is expanded and negative values refer to the cell compressed, V_0 is the cell volume at $P = 0$ and $T = 0$. From Fig. 6(a), we can see that the $(V - V_0)/V_0$ decreases with pressure increasing and the rate of decrease is very fast at 2500 K, indicating that the structure of NbN expands much more easily with the temperature rising. But the expanding effect is restrained when $P > 4.39$ GPa, $T < 2500$ K. Figure 6(b) shows

the $(V-V_0)/V$ increases with temperature rising and the rate of increase is very prominent at low pressure. That is to say, the structure of NbN expands easily at high temperature at low pressure. However, the expanding effect is suppressed and the variation is moderate with increasing pressure. These results are consistent with the scenarios in Figs. 2(a) and 2(b). Thus, we can obtain a result that the influences of temperature and pressure on the crystal cell are opposite.

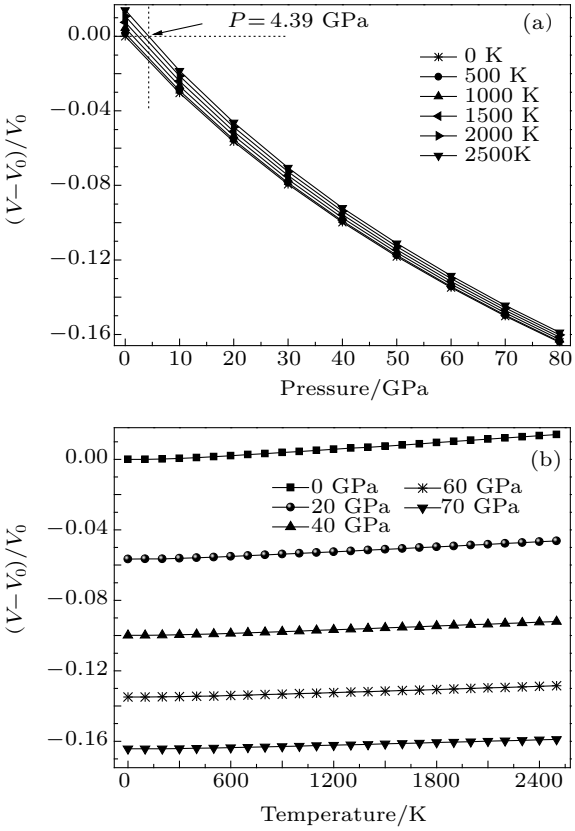


Fig. 6. Values of $(V-V_0)/V$ versus pressure P at different temperatures (a) and versus temperature T at different pressures (b), where V is the cell volume at $P=0$ and $T=0$.

The heat capacity of crystal is an old but interesting research topic in condensed matter physics.[57,58] Knowledge of the heat capacity of the substance not only provides an essential insight into its vibrational properties, but also possesses many applications. Two well-known limiting cases are correctly predicted by the standard elastic continuum theory.[58] At high temperature, the constant-volume heat capacity C_V tends to the Dulong–Petit limit; while at sufficiently low temperature, C_V is proportional to T^3.[59] At intermediate temperatures, however, the temperature dependence of C_V is governed by the details of vibration of the atoms and has long been determined only experimentally. Figure 7(a) shows the values of heat capacity C_V of NbN at different temperatures and pressures. As temperature increases, the heat capacity C_V increases at different pressures, while the increase gradually slows down. Due to the anharmonic approximation of the Debye model, C_V increases sharply with temperature rising when $T < 400$ K. However, when temperature goes up to 400 K the anharmonic effect on C_V is suppressed, and C_V tends to the Dulong–Petit limit (≈ 49.59 J·mol^{-1}·K^{-1}) gradually, which is common to all solids at high temperatures.

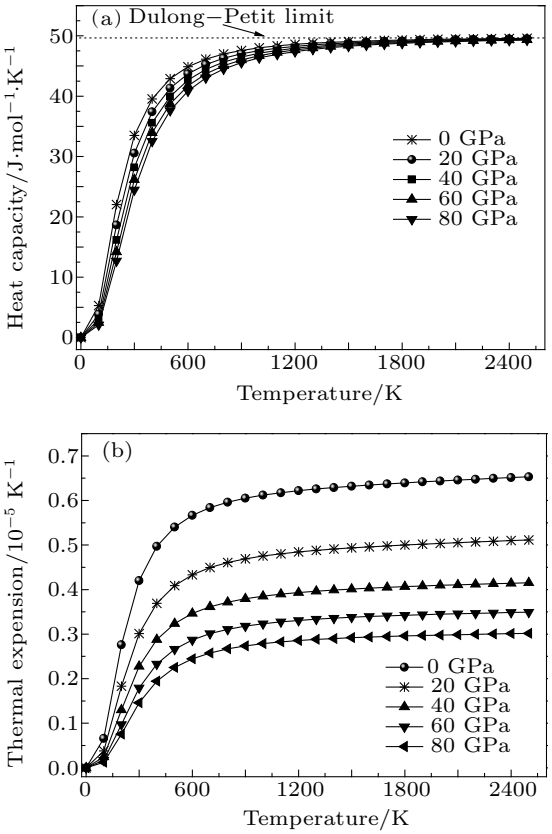


Fig. 7. (a) Curves of heat capacity (a) and thermal expansion (b) versus temperature at pressures in a range of 0 GPa–80.4 GPa

The curves of thermal expansion coefficient α versus temperature are plotted in Fig. 7(b) at different pressures. Obviously, at low temperature, α increases sharply, and then the tendency to increase becomes weaker at high temperature. At a given temperature, the higher the pressure, the smaller the thermal expansion is, which is absolutely consistent with the scenario in Fig. 7(a). While at $P = 80.4$ GPa, $T > 600$ K, α hardly changes anymore, indicating that high pressure suppresses thermal expansion effectively. At a

certain temperature, as pressure P increases, the thermal expansion coefficient α decreases. Finally, we predict that the thermal expansion coefficient α of NbN is about 4.20×10^{-6}/K at 300 K and 0 GPa.

4. Conclusions

The elastic and thermodynamic properties at different pressures and temperatures are investigated by the plane-wave pseudopotential density functional theory with CASTEP code. The equilibrium lattice parameters are consistent with the experimental data and other theoretical calculations. Temperature causes unobvious variation of the shear wave along the {100} and {110} planes, whereas pressure makes the shear change more substantially along the {110} plane than along the {100} plane. The high-pressure (80.4 GPa) longitudinal and shear-wave velocities for NbN differ by 22.8% and 9.3% as compared with those at zero-pressure. It is found that NbN is highly anisotropic in both longitudinal and shear-wave velocities. Both at zero pressure and high pressure, P waves are fastest along direction [100] and S waves are fastest along direction [110]. The thermodynamic properties are investigated by the quasi-harmonic Debye model. At sufficiently low temperature, C_V is proportional to T^3. At intermediate temperatures, however, the dependence of temperature towards C_V is governed by the details of vibration of the atoms. At high temperature, the heat capacity C_V is close to the Dulong–Petit limit (≈ 49.59 J·mol^{-1}·K^{-1}). The thermal expansion coefficient α of NbN is predicted to be about 4.2×10^{-6}/K at 0 GPa and 300 K.

References

[1] Toth L E 1971 *Transition Metal Carbides and Nitrides* (New York: Academic Press)

[2] Chhowalla M and Unalan H E 2005 *Nat. Mater.* **4** 317

[3] McMillan P F 2002 *Nat. Mater.* **1** 19

[4] Zerr A, Miehe G and Riedel R 2003 *Nat. Mater.* **2** 185

[5] Jhi S H, Ihm J, Louie S G and Cohen M L 1999 *Nature* **399** 132

[6] Chen X J, Struzhkin V V, Wu Z G, Somayazulu M, Qian J, Kung S, Christense A N, Zhao Y S, Cohen R E, Mao H K and Hemley R J 2005 *PNAS* **102** 3198

[7] Wu Z G, Chen X J, Struzhkin V V and Cohen R E 2005 *Phys. Rev.* B **71** 214103

[8] Chen Z W, Gu M X, Sun C Q, Zhang X Y and Liu R P 2007 *Appl. Phys. Lett.* **91** 061905

[9] Jhi S H, Louie S G, Cohen M L and Morris J W Jr 2001 *Phys. Rev. Lett.* **87** 075503

[10] Zhang R F, Sheng S H and Veprek S 2007 *Appl. Phys. Lett.* **91** 031906

[11] Zhang R F, Sheng S H and Veprek S 2007 *Appl. Phys. Lett.* **90** 191903

[12] Liao T, Wang J Y and Zhou Y C 2006 *Phys. Rev.* B **73** 214109

[13] Amriou T, Bouhafs B, Aourag H, Khelifa B, Bresson S and Mathieu C 2003 *Physica* B **325** 46

[14] Wang C, Wen M, Su Y D, Xu L, Qu C Q, Zhang Y J, Qiao L, Yu S S, Zheng W T and Jiang Q 2009 *Solid State Commun.* **149** 725

[15] Wang Z, Terai H, Kawakami A and Uzawa Y 1999 *Appl. Phys. Lett.* **75** 701

[16] Suzuki K, Miki S, Wang Z, Kobayashi Y, Shiki S and Ohkubo M 2008 *J. Low Temp. Phys.* **151** 766

[17] Blanco M A, Francisico E and Luaña V 2004 *Comput. Phys. Commun.* **158** 57

[18] Vanderbilt D 1990 *Phys. Rev.* B **41** 7892

[19] Perdew J P, Burke K and Ernzerhof M 1996 *Phys. Rev. Lett.* **77** 3865

[20] Pack J D and Monkhorst H J 1977 *Phys. Rev.* B **16** 1748

[21] Segall M D, Lindan P J D, Probert M J, Pickard C J, Hasnip P J, Clark S J and Payne M C 2002 *J. Phys.*: *Condens. Matter* **14** 2717

[22] Milman V, Winkler B, White J A, Packard C J, Payne M C, Akhmatskaya E V and Nobes R H 2000 *Int. J. Quantum Chem.* **77** 895.

[23] Birch E D 1986 *J. Geophys. Res.* **91** 4949

[24] Isaev E I, Simak S I, Abrikosov I A, Ahuja R, Vekilov Yu Kh, Katsnelson M I, Lichtenstein A I and Johansson B 2007 *J. Appl. Phys.* **101** 123519

[25] Villars P and Calvet L D 1985 *Pearson's Handbook of Crystallographic Data for Intermetallic Phases* (Metals Park, OH: American Society for Metals)

[26] Stampfl C, Mannstadt W, Asahi R and Freeman A J 2001 *Phys. Rev.* B **63** 155106

[27] Grossman J C, Mizel A, Côté M, Cohen M L and Louie S G 1999 *Phys. Rev.* B **60** 6343

[28] Guillermet A F, Häglund J and Grimvall G 1993 *Phys. Rev.* B **48** 11673

[29] Guillermet A F, Häglund J and Grimvall G 1992 *Phys. Rev.* B **45** 11557

[30] Häglund J, Grimvall G, Jarborg T and Guillermet A F 1991 *Phys. Rev.* B **43** 14400

[31] Hart G L W and Klein B M 2000 *Phys. Rev.* B **61** 3151

[32] Kim J O, Achenbach J D, Mirkarimi P B, Shinn M and Barnett S A 1992 *J. Appl. Phys.* **72** 1805

[33] Chen X J, Struzhkin V V, Wu Z G, Somayazulu M, Qian J, Kung S, Christensen A N, Zhao Y S, Cohen R E, Mao H K and Hemley R J 2005 *Proc. Natl. Acad. Sci. USA* **102** 3198

[34] Alfonso J E, Buitrago J, Torres J, Marco J F and Santos B 2010 *J. Mater. Sci.* **45** 5528

[35] Nye J F 1985 *Physical Properties of Crystals* (Oxford: Clarendon) p. 329

[36] Wentzcovitch R M, Ross N L and Price G D 1995 *Physics of Earth and Planetary Interiors* **90** 101

[37] Sin'ko G V and Smirnow N A 2002 *J. Phys.*: *Condens. Matter* **14** 6989

[38] Callenås A, Johansson L I, Christensen A N, Schwarz K and Blaha P 1985 *Phys. Rev.* B **32** 575

[39] Zha C S, Mao J K and Hemley R J 2000 *Proc. Natl. Acad. Sci. USA* **97** 13494

[40] Wang J H, Li J, Yip S, Phillpot S and Wolf D 1995 *Phys. Rev.* B **52** 12627

[41] Schreiber E, Anderson O L and Soga N 1973 *Elastic Constants and Their Measurements* (New York: McGraw-Hill)

[42] Lu L Y, Cheng Y, Chen X R and Zhu J 2005 *Physica* B **370** 236

[43] Anderson O L 1963 *J. Phys. Chem. Solids* **24** 909

[44] Landau L D and Lifschitz E M 1980 *Theory of Elasticity, Course of Theoretical Physics* (New York: Pergamon Press)

[45] Maradudin A A, Montroll E W, Weiss G H and Ipatova I P 1971 *Theory of Lattice Dynamics in the Harmonic Approximation* (New York: Academic Press)

[46] Blanco M A, Pendás A M, Francisco E, Recio J M and Franco R 1996 *J. Mol. Struct.* **368** 245

[47] Flórez M, Recio J M, Francisco E, Blanco M A and Pendás A M 2002 *Phys. Rev.* B **66** 144112

[48] Francisco E, Recio J M, Blanco M A and Pendás A M 1998 *J. Phys. Chem.* **102** 1595

[49] Francisco E, Blanco M A and Sanjurjo G 2001 *Phys. Rev.* B **63** 094107

[50] Poirier J P 2000 *Introduction to the Physics of the Earth's Interior* (Oxford: Cambridge University Press) p. 11

[51] Wentzcovitch R M, Chang K J and Cohen M L 1986 *Phys. Rev.* B **34** 1071

[52] Yu J X, Fu M, Ji G F and Chen X R 2009 *Chin. Phys.* B **18** 2690

[53] Cheng Y, Lu L Y, Jia O H and Chen X R 2008 *Chin. Phys.* B **17** 1355

[54] Chen D, Chen J D, Zhao L H, Wang C L, Yu B H and Shi D H 2009 *Chin. Phys.* B **18** 738

[55] Zhang Z J, Wang F, Zheng Z, Wang J J, An X Y, Liao G and Ren W Y 2010 *Physica* B **406** 737

[56] Zhai H C, Li X F, Du J Y and Ji G F 2012 *Chin. Phys.* B **21** 057102

[57] Einstein A and Ann 1907 *Ann. Phys.* **22** 180

[58] Nernst W, Lindemann A F, Elektrochem Z and Angew 1977 *Phys. Chem.* **17** 817

[59] Petit A T and Dulong P L 1819 *Ann. Chim. Phys.* **10** 395